Dalton Transactions

Accepted Manuscript

ROYAL SOCIETY OF CHEMISTRY

www.rsc.org/dalton

Influence of ionic liquids on the syntheses and structures of Mn(II) coordination polymers based on multidentate N-heterocyclic aromatic ligand and bridging carboxylate ligands

Jian-Hua Qin,[a,b] Hua-Rui Wang,[a,b] Qi Pan,[a] Shuang-Quan Zang,[a] Hongwei Hou,*[a] and Yaoting Fan[a]

Received (in XXX, XXX) Xth XXXXXXXXX 20XX, Accepted Xth XXXXXXXXX 20XX
DOI: 10.1039/b000000x

Seven Mn(II) coordination polymers, namely $\{[Mn_2(ptptp)Cl_2(H_2O)_3]\cdot H_2O\}_n$ (**1**), $\{[Mn(\mu\text{-}ptptp)_3]_2[Mn_3(\mu_3\text{-}Cl)]_2\}\cdot 2Cl\cdot 16H_2O$ (**2**), $\{[Mn_2(ptptp)(ip)_2(H_2O)_3]\cdot H_2O\}_n$ (**3**), $\{[Mn_2(ptptp)(5\text{-}CH_3\text{-}ip)_2(H_2O)_3]\cdot H_2O\}_n$ (**4**), $\{[Mn_4(ptptp)(5\text{-}Br\text{-}ip)_3(H_2O)_3]\cdot 4H_2O\}_n$ (**5**), $\{[Mn_2(ptptp)(Hbtc)(H_2O)_2]\cdot 2H_2O\}_n$ (**6**) and $\{[Mn_2(ptptp)(tdc)(H_2O)_2]\cdot 1.5H_2O\}_n$ (**7**), have been prepared based on multidentate N-heterocyclic aromatic ligand and bridging carboxylate ligands (H_2ptptp = 2-(5-{6-[5-(Pyrazin-2-yl)-1H-1,2,4-triazol-3-yl]pyridin-2-yl}-1H-1,2,4-triazol-3-yl)pyrazine; R-isophthalic acids, H_2ip-R: R = –H (**3**), $–CH_3$ (**4**), –Br (**5**); H_3btc = trimesic acid (**6**); H_2tdc = thiophene-2,5-dicarboxylic acid (**7**)), in order to further probe the multiple roles of [RMI]Br ionic liquids in the hydro/solvothermal synthesis (RMI = 1-alkyl-3-methylimidazolium, R = ethyl, or propyl, or butyl). The successful syntheses of complexes **2-6** suggest that in hydro/solvothermal synthesis the addition of small amount of [RMI]Br plays a crucial role. Complex **1** exhibits single right-stranded helices constructed by ptptp ligands and Mn(II) ions. Complex **2** possesses octanuclear helicate structures in which two propeller-shaped $[Mn(\mu\text{-}ptptp)_3]^{4-}$ units embrace two $[Mn_3(\mu_3\text{-}Cl)]^{5+}$ cluster cores inside. Complexes **3** and **4** are isostructural and display a 1D double chain formed by two kinds of pseudo meso-helix: $(Mn\text{-}ptptp)_n$ and $(Mn\text{-}5\text{-}R\text{-}ip)_n$. Complex **5** has a 2D structure containing 1D Mn(II) ions chains formed through carboxylates and $[ptptp]^{2-}$–*N*, *N* bridges. Complex **6** shows a 2D structure formed by meso-helix $(Mn\text{-}ptptp)_n$ and the partly deprotonated Hbtc ligands. Complex **7** features a heterochiral [2+2] coaxially nested double-helical column formed by using outer double-helices $(Mn\text{-}ptptp)_n$ as a template to encapsulate inner doubl-helices $(Mn\text{-}tdc)_n$ with opposite orientation. All complexes were characterized by elemental analysis, IR spectra, thermogravimetric analysis, single-crystal X-ray crystallography and powder X-ray diffraction. Magnetic properties of **1-7** were also investigated.

Introduction

Ionic liquids (ILs), a class of salts which are liquid at low temperature and consist of ions only, have received increasing attention as the solvent of choice for the syntheses of crystalline materials such as zeolites and coordination polymers (CPs).[1-4] Ionothermal synthesis, the use of an IL as solvent and structure directing agent (or template), provides quite different networks from those obtained by traditional hydro/solvothermal synthesis. Earlier reports showed that ILs could display several different types of behaviors, such as templating by only the cation or by both the cation and anion simultaneously, and serve as a mineralizing agent or solvent only without being occluded in the final structure, which illustrates that ILs can play multiple functions even in the same systems.[1-4] Many ILs are hygroscopic and contain a significant amount of water even after a moderate drying process.[5] Based on kinetic study of the effect of water, Tian and co-workers have found that in ionothermal synthesis the addition of small amount of water is important in determining the phase selectivity of the reaction and can increase the crystallisation rate.[6] Undoubtedly, in turn, introducing small amounts of ILs to hydro/solvothermal synthesis can also improve the synthetic conditions. Su group demonstrated the combination of hydro/solvothermal and ionothermal methods for the first time.[7] They found that small amounts of ILs could play a crucial role in the successful preparation of targeted crystalline materials and no crystalline phase appeared without ILs added. Compared to hydro/solvothermal and ionothermal synthesis, the combination of hydro/solvothermal and ionothermal methods seems to be a promising synthetic technique for the preparation of functional CPs.

Recently, we have successfully carried out the conversion from heterochiral [2+2] coaxially nested double-helical column $\{[Mn_2(ptptp)(suc)(H_2O)_2]\cdot 1.5H_2O\}_n$ to cationic spiral staircase $\{[Mn_2(ptptp)(suc)_{0.5}(H_2O)_3]\cdot Br\cdot 0.5H_2O\}_n$ stimulated by Br^- ions derived from [RMI]Br ILs (H_2ptptp = 2-(5-{6-[5-(Pyrazin-2-yl)-1H-1,2,4-triazol-3-yl]pyridin-2-yl}-1H-1,2,4-triazol-3-yl)pyrazine; H_2suc = succinic acid; RMI = 1-alkyl-3-methylimidazolium, R = ethyl, or propyl, or butyl).[8a] Further experiment research indicates that not only could the IL Br^- anion be occluded in the ultimate structure as template, but also the IL cation could exert important effects on the formation of $\{[Mn_2(ptptp)(suc)_{0.5}(H_2O)_3]\cdot Br\cdot 0.5H_2O\}_n$ despite the fact that they do not enter the final structure.[8a] These achievements inspire us to further probe the multiple roles of ILs in the hydro/solvothermal synthesis. Additionally, carboxylate-bridged Mn(II) complexes are of special interests, since such systems are known to exist at the active centers of some Mn(II)-containing

enzymes.[9] Moreover, these Mn(II)-carboxylates are well recognized from the magnetic point of view as the high-spin Mn(II) contains five unpaired electrons.[10-11]

To continue our study about the influence of [RMI]Br ILs on synthesizing Mn(II) CPs based on H_2ptptp and bridging carboxylate ligands, we select three R-isophthalic acids (H_2ip-R: R = –H, –CH_3 and –Br), trimesic acid (H_3btc) and thiophene-2,5-dicarboxylic acid (H_2tdc) as auciliary ligands in self-assembly process. In this work, we present seven Mn(II) CPs: $\{[Mn_2(ptptp)Cl_2(H_2O)_3]\cdot H_2O\}_n$ (**1**), $\{[Mn(\mu\text{-ptptp})_3]_2[Mn_3(\mu_3\text{-Cl})]_2\}\cdot 2Cl\cdot 16H_2O$ (**2**), $\{[Mn_2(ptptp)(ip)_2(H_2O)_3]\cdot H_2O\}_n$ (**3**), $\{[Mn_2(ptptp)(5\text{-}CH_3\text{-ip})_2(H_2O)_3]\cdot H_2O\}_n$ (**4**), $\{[Mn_4(ptptp)(5\text{-Br-ip})_3(H_2O)_3]\cdot 4H_2O\}_n$ (**5**), $\{[Mn_2(ptptp)(Hbtc)(H_2O)_2]\cdot 2H_2O\}_n$ (**6**), and $\{[Mn_2(ptptp)(tdc)(H_2O)_2]\cdot 1.5H_2O\}_n$ (**7**). Among them, **2-6** could only be obtained in the presence of [RMI]Br. Although [RMI] cation and Br^- anion were not occluded in the ultimate structure of **2-6**, [RMI]Br played important roles in the preparation of the five complexes. Many tries to synthesize the five complexes under traditional hydro/solvothermal conditions failed. Further comparison experiments indicated that [RMI]Br played different roles in the syntheses of the five complexes. Additionally, introducing [RMI]Br into the synthesis process of **7** could obviously improve crystal yield. All these observations illustrated the addition of small amounts of ILs can change the chemistry of the solvent, which can lead to great differences in the final structure compared to hydro/solvothermal condition. Magnetic properties of **1–7** were also investigated.

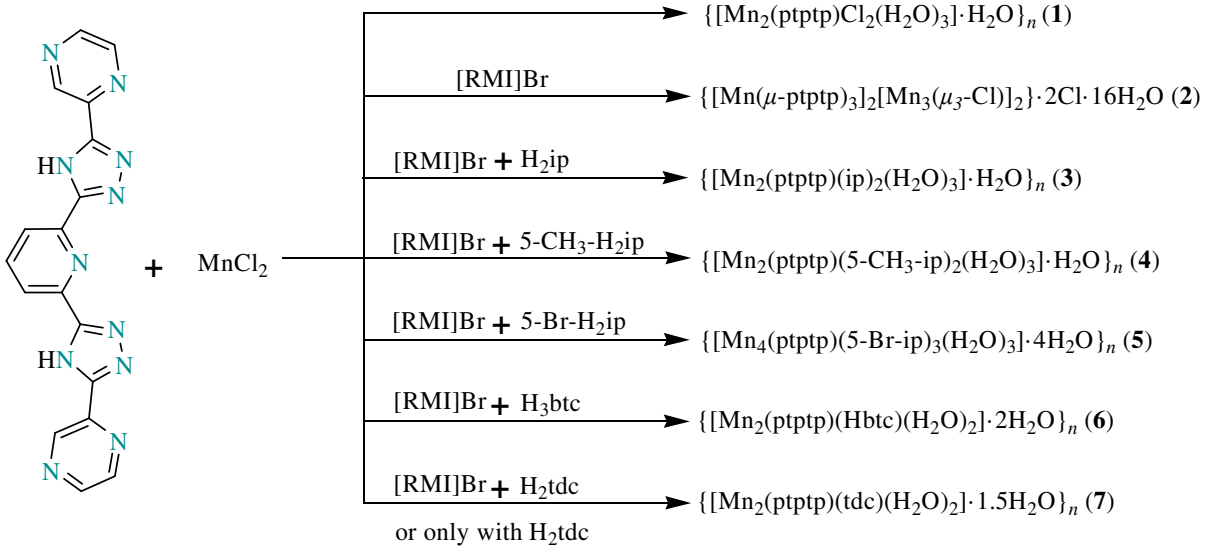

Scheme 1. Syntheses of complexes **1–7.**

Experimental section

Materials and physical measurements

All chemicals were commercially purchased and used without further purification. [RMI]Br ILs were commercially purchased from Center for Greenchemistry and Catalysis (Lanzhou Institute of Chemical Physics, Chinese Academy of Sciences). Elemental analyses for carbon, hydrogen and nitrogen were performed on a Perkin-Elmer 240 elemental analyzer. The FT-IR (4000 ~ 600 cm^{-1}) were recorded on a Bruker VECTOR 22 spectrometer. Thermogravimetric measurements were carried out in a nitrogen stream using a SDT 2960 thermal analyzer at a heating rate of 20 °C min^{-1}. Variable-temperature magnetic susceptibilities were measured using a MPMS-7 SQUID magnetometer. The powder X-ray diffraction (PXRD) patterns were recorded with a Rigaku D/Max 3III diffractometer with a scanning rate of four degrees per minute.

Syntheses of complexes 1–7.

$\{[Mn_2(ptptp)Cl_2(H_2O)_3]\cdot H_2O\}_n$ (1). A mixture of H_2ptptp[8] (0.05 mmol, 18.4 mg) and $MnCl_2\cdot 4H_2O$ (0.1 mmol, 19.8 mg) in 10 mL mixed solvent (CH_3CN/H_2O, V/V, 7:3) was placed in a 25 mL Teflon-lined stainless steel vessel, and the vessel was sealed and heated to 160 °C for 72 h. After the mixture had been cooled to room temperature at a rate of 5 °C·h^{-1}, yellow crystals of **1** were obtained with a yield of 87% (based on Mn). Anal. Calc for $C_{17}H_{17}Cl_2Mn_2N_{11}O_4$ (%): C, 32.92; H, 2.76; N, 24.84. Found: C, 32.85; H, 2.71; N, 24.74. IR (cm^{-1}, KBr): 3046 bv, 1568 w, 1552 s, 1480 s, 1367 m, 1146 s, 1080 m, 846 w, 802 w, 786 m, 443 s.

$\{[Mn(\mu\text{-ptptp})_3]_2[Mn_3(\mu_3\text{-Cl})]_2\}\cdot 2Cl\cdot 16H_2O$ (2). The process was similar to **1** except that 1 mL [RMI]Br was added. Yellow crystals of **2** were obtained with a yield of 78% (based on Mn). Anal. Calcd for $C_{102}H_{86}Cl_4Mn_8N_{66}O_{16}$ (%): C, 39.86; H, 2.82; N, 30.08. Found: 39.23; H, 2.94; N, 30.01. IR (cm^{-1}, KBr): 3421 bv, 1706 w, 1610 m, 1577 m, 1520 m, 1373 s, 1156 s, 1115 s, 1063 s, 765 m, 518 m, 444 m.

$\{[Mn_2(ptptp)(ip)_2(H_2O)_3]\cdot H_2O\}_n$ (3). A mixture of H_2ptptp (0.05 mmol, 18.4 mg), $MnCl_2\cdot 4H_2O$ (0.2 mmol, 39.6 mg), H_2ip (0.2 mmol, 33.2 mg), and 1 mL [RMI]Br in 10 mL mixed solvent (CH_3CN/H_2O, V/V, 7:3) was placed in a 25 mL Teflon-lined

stainless steel vessel, and the vessel was sealed and heated to 160 °C for 72 h. After the mixture had been cooled to room temperature at a rate of 5 °C·h^{-1}, yellow crystals of **3** were obtained with a yield of 85% (based on Mn). Anal. Calc for $C_{25}H_{21}Mn_2N_{11}O_8$ (%): C, 42.09; H, 2.97; N, 21.60. Found: C, 41.93; H, 2.92; N, 21.46. IR (cm^{-1}, KBr): 3415 bv, 1607 s, 1553 s, 1442 m, 1332 s, 1190 m, 1066 m, 1023 m, 746 m, 447 m.

{[Mn$_2$(ptptp)(5-CH$_3$-ip)$_2$(H$_2$O)$_3$]·H$_2$O}$_n$ (4). The process was similar to **3** except that H_2ip was replaced by 5-CH_3-H_2ip (0.2 mmol, 35.6 mg). Yellow crystals of **4** were obtained with a yield of 82% (based on Mn). Anal. Calc for $C_{26}H_{23}Mn_2N_{11}O_8$ (%): C, 42.93; H, 3.19; N, 21.18. Found: C, 42.81; H, 3.12; N, 21.03. IR (cm^{-1}, KBr): 3426 bv, 1683 m, 1606 m, 1574 s, 1425 m, 1366 s, 1154 m, 1049 m, 780 m, 707 m, 448 w.

{[Mn$_4$(ptptp)(5-Br-ip)$_3$(H$_2$O)$_3$]·4H$_2$O}$_n$ (5). The process was similar to **3** except that H_2ip was replaced by 5-Br-H_2ip (0.2 mmol, 48.6 mg). Yellow crystals of **5** were obtained with a yield of 88% (based on Mn). Anal. Calc for $C_{41}H_{32}Br_3Mn_4N_{11}O_{19}$ (%): C, 34.14; H, 2.24; N, 10.68. Found: C, 34.47; H, 2.32; N, 10.62. IR (cm^{-1}, KBr): 3419 bv, 1608 s, 1564 s, 1370 s, 1145 w, 1033 w, 776 m, 715 m, 454 w.

{[Mn$_2$(ptptp)(Hbtc)(H$_2$O)$_2$]·2H$_2$O}$_n$ (6). The process was similar to **3** except that H_2ip was replaced by H_3btc (0.2 mmol, 42.0 mg). Yellow crystals of **6** were obtained with a yield of 65% (based on Mn). Anal. Calc for $C_{26}H_{21}Mn_2N_{11}O_{10}$ (%): C, 41.23; H, 2.79; N, 20.34. Found: C, 41.13; H, 2.72; N, 20.19. IR (cm^{-1}, KBr): 3396 bv, 1619 s, 1572 s, 1434 s, 1282 m, 1144 m, 1039 w, 755 w, 706 w, 524 w.

{[Mn$_2$(ptptp)(tdc)(H$_2$O)$_2$]·1.5H$_2$O}$_n$ (7). *First method*: The process was similar to **3** except that H_2ip was replaced by H_2tdc (0.2 mmol, 34.4 mg). Yellow crystals of **7** were obtained with a yield of 92% (based on Mn). Anal. Calc for $C_{46}H_{36}Mn_4N_{22}O_{15}S_2$ (%): C, 38.89 H, 2.55; N, 21.69. Found: C, 38.71; H, 2.31; N, 21.56. IR (cm^{-1}, KBr): 3282 bv, 2360 w, 1548 s, 1503 m, 1396 s, 1395 s, 1274 m, 1186 m, 1060 m, 857 m, 738 m, 445 s.

Second method: A mixture of H_2ptptp (0.05 mmol, 18.4 mg), $MnCl_2·4H_2O$ (0.2 mmol, 39.6 mg) and H_2tdc (0.2 mmol, 34.4 mg) in 10 mL mixed solvent (CH_3CN/H_2O, V/V, 7:3) was placed in a 25 mL Teflon-lined stainless steel vessel, and the vessel was sealed and heated to 160 °C for 72 h. Yellow crystals of **7** were obtained with a yield of 76% (based on Mn), which is lower than that in the presence of [RMI]Br.

X-ray crystallography

Single crystal X-ray diffraction analyses of **1**, **2**, **3**, **4**, **5**, and **6** were collected on a Rigaku Saturn 724 CCD diffractomer (Mo-Kα, λ = 0.71073 Å) at temperature of 20 ± 1 °C. The data of **7** was carried out on a Bruker SMART APEX II CCD diffractometer equipped with a graphite monochromated Mo *K*α radiation (*λ* = 0.71073 Å) by using *φ*/*ω* scan technique at room temperature. The structures were solved by direct methods with SHELXS-97[12] and refined by the full-matrix least-squares method on F^2 with anisotropic thermal parameters for all non-H atoms (SHELXL-97)[13]. The empirical absorption corrections were applied by the SADABS program.[14] The hydrogen atoms were assigned with common isotropic displacement factors and included in the final refinement by use of geometrical restrains. There are large solvent accessible void volumes in the crystals of both **2** and **5** which are occupied by highly disordered free water molecules. No satisfactory disorder model could be achieved, and therefore the SQUEEZE program implemented in PLATON was used to remove these electron densities.[15] The numbers of water molecules were obtained by element analyses and TGA. The crystallographic data and selected bond lengths and angles for **1**–**7** are listed in Table 1 and Table S2 in ESI†. Crystallographic data for the structural analyses have been deposited with the Cambridge Crystallographic Data Center. CCDC numbers for complexes **1**–**7** are 1012966–1012972, respectively.

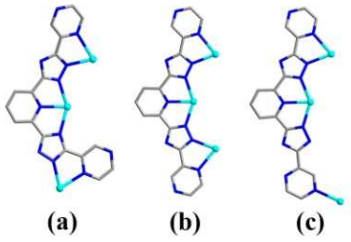

Scheme 2. Coordination modes of ptptp ligands in **1** (a), **2** (b), **3** (c), **4** (c), **5** (b), **6** (a) and **7** (b). Color code: C gray, N blue, Mn turquoise.

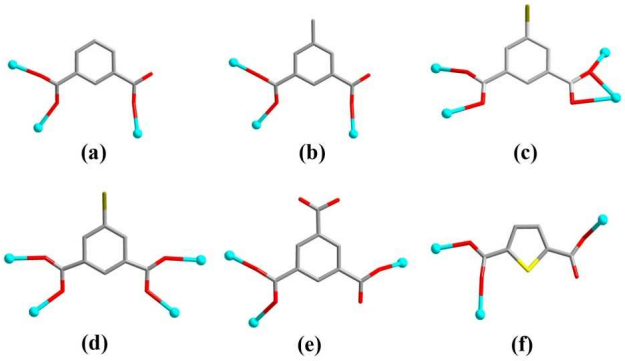

Scheme 3. Coordination modes of bridging carboxylate ligands in **3** (a), **4** (b), **5** (c, d), **6** (e) and **7** (f). Color code: C gray, O red, Mn turquoise, Br dark yellow, S yellow.

Results and Discussion

Descriptions of Crystal Structures

{[Mn$_2$(ptptp)Cl$_2$(H$_2$O)$_3$]·H$_2$O}$_n$ (1). X-ray crystal structure analysis reveals that **1** crystallizes in the monoclinic system with *P*2(1) space group. As shown in Fig. 1a, the asymmetric unit of **1** possesses two crystallographically unique Mn(II) ions, one completely deprotonated ptptp ligand, two Cl^- ions, three coordinated water molecules and one free water molecule. The Mn1 ion is coordinated by two terminal bidentate binding sites of two ptptp ligands and one Cl^- ion as well as one coordinated water molecule, resulting in a distorted octahedral {N_4ClO} coordination geometry. The angle between the planes defined by the two N–Mn–N chelate rings at Mn1 ion is 82.148°, and the bite angle of each bidentate binding unit is 71.85(12) and 73.46(13)°, respectively. The Mn2 ion is embedded in the central tridentate binding site of ptptp ligand, along with one Cl^- ions and two coordinated water molecules to complete a distorted

octahedral $\{N_3ClO_2\}$ coordination geometry. Within this assembly, the adjacent Mn···Mn distance is 4.8946(8) Å (Mn1–Mn2).

The interesting feature of **1** is the presence of right-stranded helices in the structure. As depicted in Figure 1b, the ptptp ligands adopt *syn-anti* coordination mode (Scheme 2a) and bridge adjacent Mn(II) ions to form right-stranded helix. The pitch of the single-stranded helix running along the *b* axis is equal to the length of the *b* axis. The occurrence of helical strands in **1** is attributable to the versatile coordination modes of ptptp ligand. Adjacent right-stranded helices are connected by the interactions of face-to-face π···π stacking between terminal pyrazine rings to give rise to 2D supramolecular network (Fig. 1b). Furthermore, these 2D layers are combined through O–H···Cl hydrogen bonds between coordinated H_2O molecules and Cl2 atoms to generate a 3D supramolecular framework (Fig. S1 and Table S3 in ESI†).

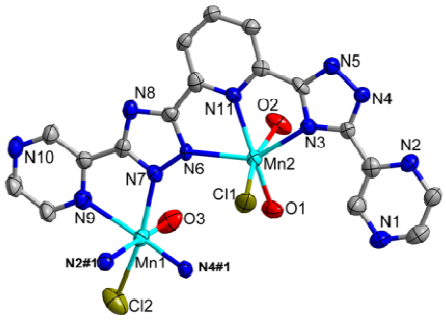

(a)

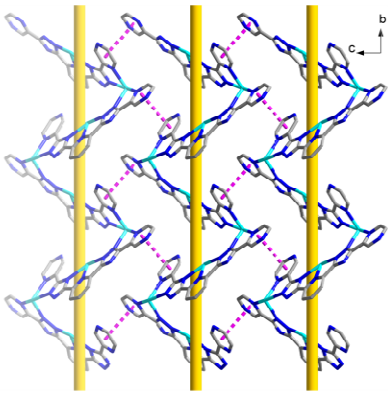

(b)

Fig. 1 (a) View of local coordination environment of Mn(II) ions in **1**. Symmetry codes: #1 -x+1, y+1/2, -z+1. (b) View of right-stranded helices and π···π stacking between terminal pyrazine rings. H atoms are omitted for clarity.

$\{[Mn(\mu\text{-ptptp})_3]_2[Mn_3(\mu_3\text{-Cl})]_2\}\cdot 2Cl\cdot 16H_2O$ (2). Complex **2** consists of eight Mn(II) ions, six ptptp ligands, four Cl^- ions and sixteen lattice H_2O molecules, as confirmed by charge balance and TG. The structure of the triple-stranded helicate **2** can be viewed as two $[Mn_3(\mu_3\text{-Cl})]^{5+}$ cluster cores wrapped by two terminal $[Mn(\mu\text{-ptptp})_3]^{4-}$ units, and the whole tricationic helicate is balanced by two free Cl^- ions (Fig. 2a and 2b). Each Mn(II) ion in $[Mn_3(\mu_3\text{-Cl})]^{5+}$ cluster core has a $\{N_5Cl\}$ coordination environment in which it is fixed by central tridentate binding site and terminal bidentate binding site of different ptptp ligand and Cl^- ion, resulting in an octahedral coordination geometry. The two Mn(II) ions in two $[Mn(\mu\text{-ptptp})_3]^{4-}$ units, located at the extremities of the helical cluster, have octahedral $\{N_6\}$ donor sets through the coordination of three bidentate ligand binding sites. Eight Mn(II) ions form a distorted bicapped trigonal antiprism polyhedron, in which two offset Mn_3 triangles bridged by μ_3-Cl atoms define the antiprism, and the rest two Mn ions locate above and below the triangle faces. Each ptptp ligand coordinates to three Mn(II) ions by using its two bidentate and one tridentate binding sites (Scheme 2b). Three pairs of ligands with strong offset face-to-face π···π stacking interactions wrap the Mn_8 polyhedron in a propeller-like form. The two apical Mn(II) ions possess the same chirality due to a screwed arrangement of the ptptp ligands, resulting in a triple-stranded *M*(Λ, Λ) or *P*(Δ, Δ) helicate. In the crystal packing left-handed and right-handed triple-stranded helicate enantiomers stack alternatively through π···π interactions and hydrogen bonds, resulting in a racemate (Fig. 2c).

There are some examples of cluster helicates, in which a $[M^{2+}{}_3(\mu_3\text{-O})]^{4+}$ (M^{2+} = Zn^{2+}, Cd^{2+}, Mn^{2+}, Fe^{2+}) core wrapped by two terminal $[M^{2+}(\mu\text{-L})_3]^{n-}$ units by using bidentate–bidentate or bidentate–tridentate–bidentate segmental ligands.[16] Recently, Tong's group has reported a new series of cluster helicates by introducing a $[M^{2+}{}_3(\mu_3\text{-X})]^{5+}$ (M^{2+} = Mn^{2+}, X = Cl; M^{2+} = Cd^{2+}, X = Br or I), a bigger halogen atom taking the central position instead of the O atom.[17] Note that a Mn complex $[\{Mn(\mu\text{-L})_3\}\{Mn_3(\mu_3\text{-Cl})\}_2](ClO_4)_2\cdot 2MeOH\cdot 6H_2O$ (L = 2,6-bis[5-(2-pyridinyl)-1H-triazol-3-yl]pyridine), shows a similar triple-stranded structure to that of **2**.[17] A further comparison of the two Mn complexes indicates that the pyrazine rings in **2** probably provide hydrogen bonds with free water molecules which may lead to different stacking arrangement. It should be noted that quite limited examples of cluster helicates have been reported because of the lack of an efficient synthetic strategy.

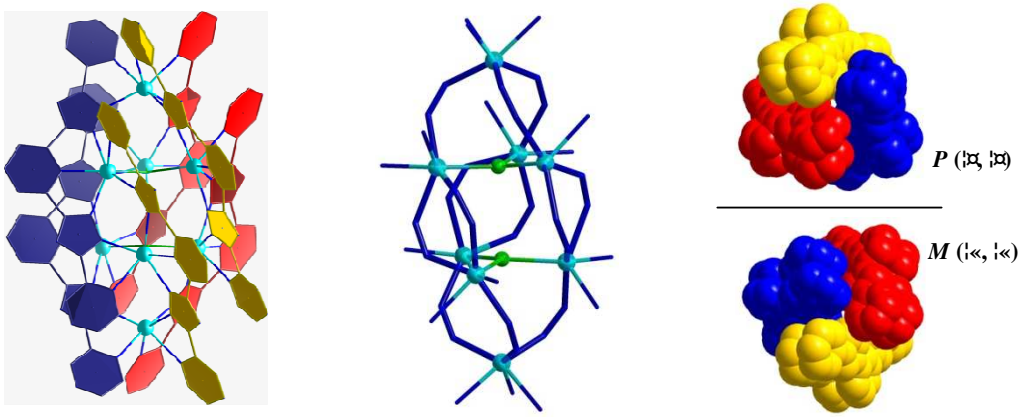

(a) (b) (c)

Fig.2 (a) Ball-and-stick representation of the ΛΛ-configurational helicate. (b) The coordination environments and bridging pathways of Mn(II) ions. (c) Space-filling representation of the two enantiomers present in **2**. H atoms are omitted for clarity.

{[Mn_2(ptptp)(ip)$_2$(H_2O)$_3$]·H_2O}$_n$ (3) and {[Mn_2(ptptp)(5-CH_3-ip)$_2$(H_2O)$_3$]·H_2O}$_n$ (4). X-ray crystal structure analyses reveals that **3** and **4** are isostructural and crystallize in the monoclinic system with *P*2(1)/c space group. Therefore, only the structure of **4** is described in detail. As shown in Fig. 3a, the asymmetric unit of **4** contains two crystallographically unique Mn(II) ions, one completely deprotonated ptptp ligand, one 5-CH_3-ip ligand, three coordinated water molecules and one free water molecule. The Mn1 ion is located in the central tridentate binding site of ptptp ligand, along with one terminal pyrazine nitrogen atom from another ptptp ligand, one oxygen atom of one 5-CH_3-ip ligand and one coordinated water molecule to give a distorted octahedral {N_4O_2} coordination geometry. The Mn2 ion lies in the terminal bidentate binding sites of one ptptp ligand and is coordinated by two oxygen atoms from two 5-CH_3-ip ligands and two coordinated water molecules, to finish a distorted octahedral {N_2O_4} coordination geometry. The bite angle of the bidentate binding unit at Mn2 ion is 70.98(16)°. Within this assembly, the adjacent Mn···Mn distances are 4.5165(17) Å (Mn1–Mn2).

The interesting feature of **4** is that the linkages between the Mn(II) ions, ptptp and 5-CH_3-ip ligands form a 1D double chain constructed from two kinds of pseudo meso-helix: (Mn-ptptp)$_n$ and (Mn-5-CH_3-ip)$_n$ (Fig. 3b). Each ptptp ligand connects three Mn(II) ions by using its one bidentate and one tridentate binding sites as well as one pyrazine nitrogen atom to form a meso-helix (Mn-ptptp)$_n$ (Scheme 2c). The 5-CH_3-ip ligand adopts μ_2-η^1:η^1 and μ_1-η^1:η^0 coordinated modes for two carboxylic groups (Scheme 3b), thus giving rise to the other meso-helix (Mn-5-CH_3-ip)$_n$. These two kinds of meso-helix share the same Mn ions and collaborate with each other to form a 1D double chain. The 1D double chains are linked by O–H···O hydrogen bonds between coordinated H_2O molecules to generate 2D layers, which are further connected by the interactions of face-to-face π···π stacking (4.0234(7) Å) between adjacent ptptp ligands to give rise to a 3D supramolecular architecture (Fig. S2 and Table S3 in ESI†).

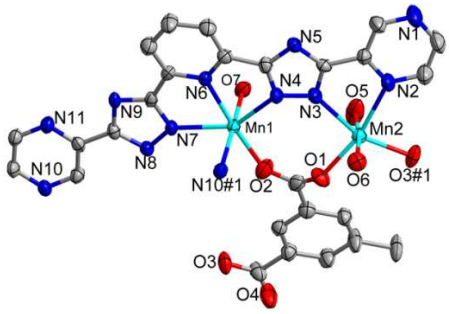

(a)

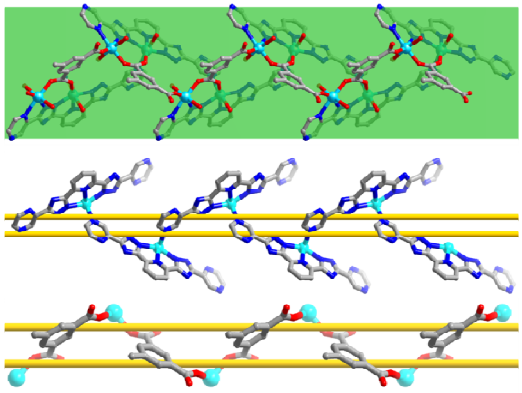

(b)

Fig. 3 (a) View of local coordination environment of Mn(II) ions in **4**. Symmetry codes: #1 x, -y+3/2, z+1/2. (b) View of 1D double chain constructed from two kinds of pseudo meso-helix: (Mn-ptptp)$_n$ and (Mn-5-CH_3-ip)$_n$. H atoms are omitted for clarity.

{[Mn_4(ptptp)(5-Br-ip)$_3$(H_2O)$_3$]·$4H_2O$}$_n$ (5). Complex **5** crystallizes in the triclinic space group *P*-1 and consists of five crystallographically unique Mn(II) ions, one completely

deprotonated ptptp ligand, three 5-Br-ip ligands, three coordinated water molecules and four free water molecules. While Mn2, Mn3 and Mn4 ions are in a general position, Mn1 and Mn5 ions are both located at crystallographic inversion sites. As illustrated in Fig. 4a, all the Mn(II) ions exhibit hexacoordinated distorted octahedral coordination geometry. The Mn1 and Mn5 ions are both coordinated by six carboxylate oxygen atoms from six different 5-Br-ip ligands. The Mn2 and Mn4 ions lie in the two terminal bidentate binding sites of one ptptp ligand collaborated with four carboxylate oxygen atoms from three different 5-Br-ip ligands to give a $\{N_2O_4\}$ geometry. The bite angle of the bidentate binding unit at Mn2 and Mn4 ions are 72.77(13)° and 72.94(14)°, respectively. The Mn3 ion is fixed in the central tridentate binding site of ptptp ligand and binded by three coordinated water molecules to furnish a $\{N_3O_3\}$ geometry. Within this assembly, the adjacent Mn···Mn distances are 3.4586(10) Å for Mn1–Mn2, 4.5820(12) Å for Mn2–Mn3, 4.6079(12) Å for Mn3–Mn4 and 3.4656(10) Å for Mn4–Mn5.

The two carboxylate groups of completely deprotonated 5-Br-ip ligands adopt different bridging modes (μ_2-η^1:η^1 and μ_2-η^2:η^1 Scheme 3c and 3d) with Mn(II) ions, resulting in the formation of Mn(II)-carboxylate trinuclear clusters intersperse through the 2D layer, which are represented as polyhedrons in light blue (Fig. 4b). Each Mn(II)-carboxylate trinuclear cluster can be regarded as a SBU. As shown in Figure 4b, these SBUs are sustained by rigid phenyl rings of 5-Br-ip ligands to construct a 2D coordination layer. By utilizing its two terminal bidentate binding sites (Scheme 2b), each ptptp ligand connects two neighbouring Mn(II)-carboxylate trinuclear clusters along *c* axis. And these ptptp ligands arrange below and above *c* axis alternately (Fig. 4c). In order to make the structure look more intuitively, we define the Mn(II)-carboxylate trinuclear clusters as capsules in light blue, ptptp ligands as blue sticks and 5-Br-ip as light green sticks, and the simplified sketch of the whole 2D structure is shown in Fig. 4d. Adjacent 2D layers are connected by the interactions of face-to-face π···π stacking between terminal pyrazine rings and triazole rings to give rise to a 3D supramolecular network (Fig. S3 in ESI†).

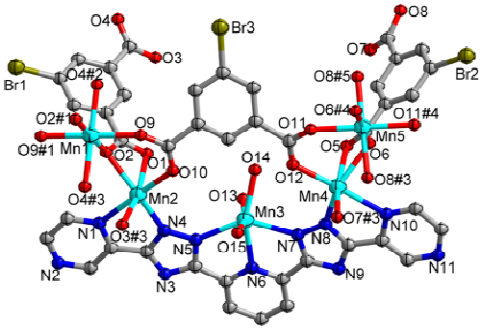

(a)

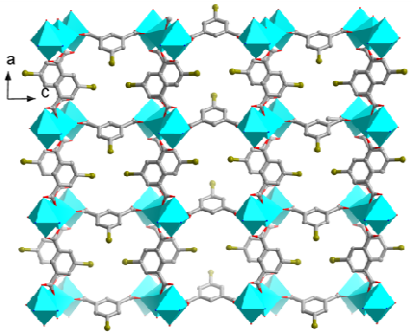

(b)

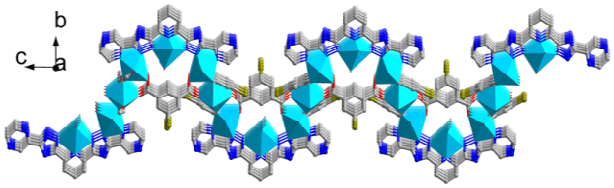

(c)

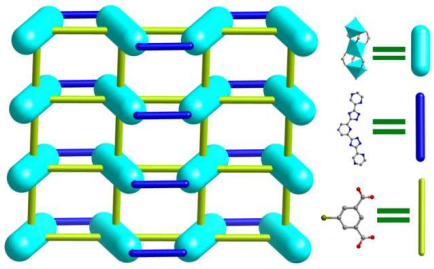

(d)

Fig. 4 (a) View of local coordination environment of Mn(II) ions in **5**. Symmetry codes: #1 -x+1, -y+1, -z+1; #2 -x, -y+1, -z+1; #3 x+1, y, z; #4 -x+1, -y+1, -z; #5 -x, -y+1, -z. (b) View of 2D layer constructed from 5-Br-ip ligands. (c) View of 2D layer constructed from 5-Br-ip ligands and ptptp ligands. (d) The simplified sketch of the whole 2D structure. H atoms are omitted for clarity.

$\{[Mn_2(ptptp)(Hbtc)(H_2O)_2]\cdot 2H_2O\}_n$ (6). Complex **6** crystallizes in the monoclinic system with *P*2(1)/*c* space group and consists of two crystallographically unique Mn(II) ions, one completely deprotonated ptptp ligand, one partly deprotonated trimesic acid (Hbtc), two coordinated water molecules and two free water molecules (Fig. 5a). The Mn1 ion is chelated by two terminal bidentate binding sites of two ptptp ligands along with two oxygen atoms from two Hbtc ligands to give a distorted octahedral $\{N_4O_2\}$ coordination geometry. The Mn2 ion is located in the central tridentate binding site of ptptp ligand and is linked by one oxygen atom of one Hbtc ligand and two coordinated water molecules to finish a distorted octahedral $\{N_3O_3\}$ coordination geometry. The bite angle of the bidentate binding unit at Mn1 ion is 72.91(11)° and 70.15(12)°. Within this assembly, the adjacent Mn···Mn distances are 4.3054(8) Å (Mn1–Mn2).

The interesting feature of **6** is that the linkages between the Mn(II) ions, ptptp ligands form a meso-helix: $(Mn\text{-}ptptp)_n$ (Fig. 5b). The ptptp ligands coordinates with Mn(II) ions by using terminal bidentate binding sites and central tridentate binding sites (Scheme 2a) to afford a fascinating mesohelical chain with left- and right-handed helical loops in one single strand along the *c* axis. The helical pitch is 19.287 Å, corresponding to the length of the *c* axis. The partly deprotonated Hbtc ligand adopts μ_2-η^1:η^1 and μ_1-η^1:η^0 coordinated modes to coordinate with Mn(II) ions (Scheme 3e), thus connecting adjacent meso-helix $(Mn\text{-}ptptp)_n$ to give rising to a 2D puckered layer (Fig. 5b). Two neighboring 2D layers are combined by π···π stacking between terminal pyrazine rings and central pyridine rings to generate a 2D supramolecular bilayer structure (Fig. S4). Furthermore, adjacent bilayers are extended to a 3D supramolecular framework by connection of O–H···N hydrogen bonds between O atoms of carboxyl and N atoms from terminal pyrazine rings (Fig. S4 and Table S3 in ESI†).

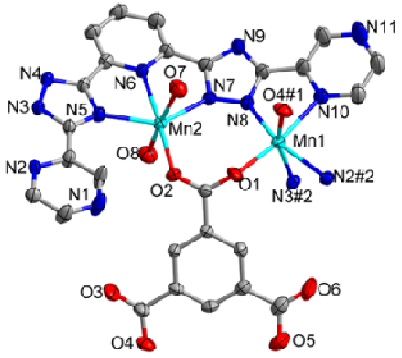

(a)

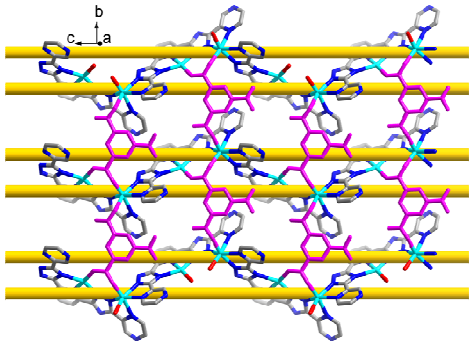

(b)

Fig. 5 (a) View of local coordination environment of Mn(II) ions in **6**. Symmetry codes: #1 x, y+1, z; #2 x, -y+3/2, z-1/2. (b) View of the 2D puckere layer and meso-helix $(Mn\text{-}ptptp)_n$. H atoms are omitted for clarity.

$\{[Mn_2(ptptp)(tdc)(H_2O)_2]\cdot 1.5H_2O\}_n$ (7). Complex **7** crystallizes in the high symmetry tetragonal space group $P4_2/n$. The asymmetric unit of **7** contains two crystallographically independent Mn(II) ions, one ptptp ligand, one tdc ligand, two coordinated water molecules, as well as one and a half free water molecules (Fig. 6a). The apical Mn1 ion is coordinated by two terminal bidentate binding sites of two ptptp ligands and two carboxylate oxygen atoms of two tdc ligands, resulting in a distorted octahedral $\{N_4O_2\}$ coordination geometry. The angle between the planes defined by the two N–Mn–N chelate rings at Mn1 ion is 80.63°, and the bite angle of each bidentate binding unit is 72.08(12) and 73.16(12)°, respectively. The Mn2 ion is embedded in the central tridentate binding site of ptptp ligand, along with one carboxylate oxygen atom from tdc ligand and two coordinated water molecules to complete a distorted octahedral $\{N_3O_3\}$ coordination geometry. The most striking feature of **7** is that the linkages between the Mn(II) ions, ptptp and tdc ligands form a heterochiral [2+2] nested double-helical column constructed from two kinds of double-helical chains in opposite orientation with the coaxial 4_2 screw axis (Fig. 6b). The Mn(II) ions are wrapped by head-to-tail ptptp ligands to form outer double-helices $(Mn\text{-}ptptp)_n$, while the Mn(II) ions are connected by tdc ligands to form inner double-helices $(Mn\text{-}tdc)_n$. The outer and inner double-helices share the same Mn ions, which brings about the same separation (*c*) between adjacent chains of each type of double-helical chains and the same pitch (2*c*). To the best of our knowledge, **7** is the second example of 1D CP that has [2+2] coaxially nested double-helical chains with the reverse chirality.[8a]

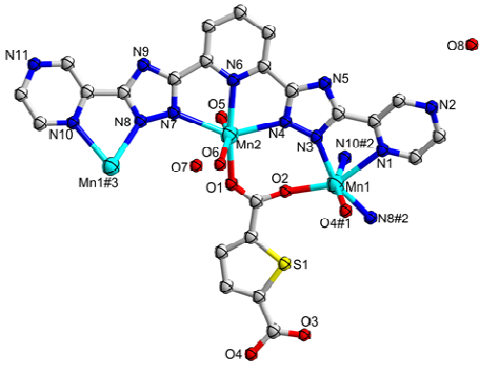

(a)

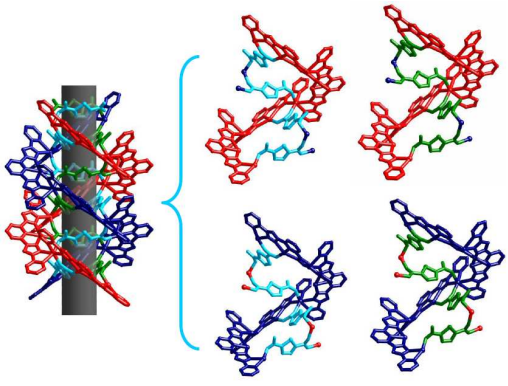

(b)

Fig. 6 (a) View of local coordination environment of Mn(II) ions in **7**. Symmetry codes: #1 y+1/2, -x+1, z-1/2; #2 -y+1, x-1/2, z-1/2; #3 y+1/2, -x+1, z+1/2. (b) Linkage between outer double-helices and inner double-helices.

The Role of ILs and Structural Diversity

As mentioned above, ILs can serve as the solvent, structure-directing agent, charge compensating agent, and can not only influence the crystal structure but also enter the material as a component. To date, much of the work on ionothermal synthesis has concentrated on the use of [RMI]Br as the solvent. To gain some insight into the reaction mechanism and optimize reaction conditions, we conducted a series of experiments to determine the effects of cation, anion and the concentration of ionic liquid separately. First, when the cation of the IL altering from $[EMI]^+$ to $[PMI]^+$ or $[BMI]^+$, **2-6** could also be successfully obtained, which may attribute to the very similar structure of the ILs' cations $[EMI]^+$, $[PMI]^+$, and $[BMI]^+$. The only difference is very slight change of crystal yield. However, when other bromide salt, NaBr, KBr, or NH4Br was selected to replace [RMI]Br, **2-6** could not be obtained. Second, when [EMI]Br was replaced by [EMI]Cl or [EMI]I to study the effects of other halogen anions, **2-6** could also not be obtained, probably due to the different nucleophilicity and/or the basicity of Cl^-, I^- and Br^- anion during the complicated crystallization process. Besides, we also tried to replaced [EMI]Br by other ILs, such as $[EMI]BF_4$, $[EMI]ClO_4$, $[EMI]CF_3SO_3$, $[EMI]PF_6$ and $[EMI]N(CF_3SO_2)_2$ in the preparation of **2-6**. Experiment result showed that only much unspecified impurities rather than any crystals could be found in this system. These ILs didn't play the same role as that [EMI]Br did. As we know, the nature of the anion plays an extremely important part in controlling the nature of the IL. One function of the anion is to control the amount of water present in the IL. The hydrophilicity order is $Br^- > BF_4^- > ClO_4^- > CF_3SO_3^- > PF_6^- > (CF_3SO_2)_2N^-$. Clearly, this change in IL chemistry on alteration of the IL anion is bound to have a significant effect on the products of any reaction carried out in such solvents. Related studies have shown that hydrophilic ILs containing small amounts of water tend to facilitate the production of framework complexes, while the hydrophobic nature of $[EMI]N(CF_3SO_2)_2$ results in poor solubilization of metal ions and organic ligands, which in turn inhibits the formation of polymeric structures.[3] Perhaps the successful synthesis of **2-6** is realized when a very hydrophilic ionic liquid is used.

Additionally, we conducted a series of experiments with different concentrations of [EMI]Br to optimize reaction conditions. The additive amount of [EMI]Br was changed as 2 mL, 1.5 mL, 0.75 mL, 0.5 mL, 0.2 mL and 0.1 mL in the preparation of **2-6**. When the additive amount was greater than 1 mL, **2-6** could also be obtained and the crystal yield had no obvious change. When the additive amount was 0.75 mL, 0.5 mL and 0.2 mL, **2-6** could be obtained with lower yield, especially when the additive amount was 0.2 mL. When the additive amount was 0.1 mL, **3-6** could still be obtained, but **2** not, and the crystal product was proved to be **1**. Above experiments show that appropriate concentration of ionic liquid (~ 1 mL) is better for the growth of single crystals with good qualities and high yields.

During the course of synthesizing complexes **2-6**, we carried out many comparison experiments to investigate the different role of [RMI]Br. First, if no [RMI]Br was introduced into the preparation of **2-6**, the ultimate crystalline products turned out to be always **1**. Second, when [RMI]Br was added, the targeted crystalline products were synthesized in good qualities and moderate yields. Further analysis shows that [RMI]Br may play different roles in the preparation of the five complexes. In **2**, [RMI]Br probably serves as a template directing agent for the formation of triple-stranded linear cluster helicate, though neither [RMI] cation nor Br^- anion is occluded into the ultimate structure. While in **3-6**, [RMI]Br perhaps serves as a mineralizing agent during the reaction process.[7] Additionally, it is worth mentioning that even introducing [RMI]Br into the synthesis process of **7**, ILs Br^- anion could not be occluded in the ultimate structure as they do in $\{[Mn_2(ptptp)(suc)_{0.5}(H_2O)_3]\cdot Br\cdot 0.5H_2O\}_n$.[8a] The steric hindrance of thiophene ring of H_2tdc probably prevents Br^- anion from being wrapped into the chiral channel formed by outer double-helices $(Mn\text{-}ptptp)_n$. The synthetic route for these Mn(II) CPs is schematically depicted in Scheme 1.

Compared with the crystal structures of **1** and **2**, obvious changes happened in the coordination mode of ptptp ligand, which further led to the conversion from right-stranded helix to triple-stranded linear cluster helicate. As for **3-6**, it can be concluded that the coordination fashions of R-isophthalic and trimesic acids play a key role in constructing their lattice architectures. Isophthalic acid and its derivatives with special conformations, such as with a 120° angle between two carboxylic groups, have been extensively used to prepare a variety of coordination polymers in virtue of the robust and versatile coordination capability of carboxylate.[18] Many efforts have conducted a systemic investigation of the 5-position substituent influence of R-isophthalic acids with different coordination-unfavourable groups, on the construction of coordination networks, based on the electronic and/or steric consideration.[19] The crystal structures of **3-6** depend on the different functional groups on 5-position. More interestingly, the altering of bridging carboxylate ligand from R-isophthalic acids (in **3-6**) to H_2tdc (in **7**) led to the formation of heterochiral [2+2] coaxially nested double-helical column (**7**), which may be attributed to the V-shaped configuration and small size of H_2tdc.

PXRD and Thermal Properties

In order to check the phase purity of **1**–**7**, the X-ray powder diffraction (XRPD) pattern was checked at room temperature. The simulated and experimental PXRD patterns of **1**–**7** are in good agreement with each other (Fig. S5 in ESI†), indicating the phase purity of the products. The differences in intensity may be due to the preferred orientation of the powder samples.

In order to characterize the complexes more fully in terms of thermal stability, their thermal behaviors were studied by thermogravimetric analysis (TGA) in a dry nitrogen atmosphere from 30 to 900 °C. The experiments were performed on samples consisting of numerous single crystals of **1**–**7** (Fig. S6 in ESI†). The TG curve of **1** shows a weight loss (11.44%) at 80-190 °C, corresponding to the loss of a lattice water molecule and three coordinated water molecules (calcd: 11.62 %). The framework of **1** begins to collapse from about 379 °C. Complex **2** displays a weight loss (9.37 %) at 40-92 °C, corresponding to the loss of sixteen lattice water molecules (calcd: 9.38 %). The removal of the organic components occurs in the range 486-613 °C. Complex **3** and **4** lose their lattice water molecules and three coordinated

waters molecules at 138-258 °C (calcd 10.09 % and expt 10.86 %) and at 57-215 °C (calcd 9.90 % and expt 10.63 %), respectively. Their frameworks begin to collapse from about 442 and 432 °C, respectively. Complex **5** exhibits a weight loss (5.05 %) at 89-227 °C, corresponding to the loss of four lattice water molecules (calcd: 4.99 %). The framework of **5** begins to collapse from about 285 °C. Complex **6** displays a weight loss (9.84 %) at 106-220 °C, corresponding to the loss of four lattice water molecules and three coordinated water molecules (calcd: 9.51 %). The framework of **6** begins to collapse from about 443 °C. Complex **7** shows a weight loss of 8.73% at 97-198°C corresponding to the release of lattice water molecules and coordinated water molecules (calcd, 8.88%). The framework of **7** begins to collapse from about 334 °C.

Magnetic Properties

The magnetic susceptibilities of **1-7** were measured in the 2-300 K temperature range, and shown as $\chi_M T$ and χ_M versus T plots in Fig. 7. As the temperature was lowered to 2 K, the $\chi_M T$ value continuously decreased, which suggests that antiferromagnetic interactions are operative in **1-7**. The Curie–Weiss datas and J/g values as well as the error for **1-7** are summarized in Table S1 in ESI†. The experimental $\chi_M T$ values of **1**, **3**, **4** and **6** at room temperature are 8.91, 8.55, 8.56 and 8.58 cm^3 K mol^{-1}, respectively, which are comparable with that expected for a noninteracting pair of Mn(II) ions with S = $^5/_2$ (8.75 cm^3 K mol^{-1}). The temperature dependence of the reciprocal susceptibilities ($1/\chi_M$) of **1**, **3**, **4** and **6** all obey the Curie–Weiss law in the range of 2-300 K with θ = –3.4 K, C = 9.09 cm^3 K mol^{-1} and $R = 1.78 \times 10^{-4}$ for **1**; θ = –6.11 K, C = 8.79 cm^3 K mol^{-1} and $R = 1.27 \times 10^{-4}$ for **3**; θ = –6.20 K, C = 8.80 cm^3 K mol^{-1} and $R = 1.28 \times 10^{-4}$ for **4**; and θ = –10.90 K, C = 8.90 cm^3 K mol^{-1} and $R = 1.75 \times 10^{-4}$ for **6**. The negative θ values indicate the presence of antiferromagnetic interactions between adjacent Mn(II) ions.

From a magnetic point of view, **1**, **3**, **4** and **6** can be considered as dinuclear ones, in which two Mn(II) ions are linked by one $[ptptp]^{2-}$–*N*, *N* bridge (in **1**) and one *syn–syn* carboxylate bridge as well as one $[ptptp]^{2-}$–*N*, *N* bridge (in **3**, **4** and **6**). In these dinuclear structures, the Mn···Mn distances are 4.8946(8) Å in **1**, 4.4900(14) Å in **3**, 4.5165(17) Å in **4**, and 4.3054(8) Å in **6**, respectively. To quantitatively evaluate the magnetic interactions in **1**, **3**, **4** and **6**, for similar binuclear Mn(II) complexes, the following equation (1) is induced using a Dirac–van Vleck–Heisenberg spin Hamiltonian $H = -JS_1S_2$. [20]

$$X_M = \frac{2Ng^2\beta^2}{kT}\frac{A}{B} \quad (1)$$

$$A = e^{2J/kT} + 5e^{6J/kT} + 14e^{12J/kT} + 30e^{20J/kT} + 55e^{30J/kT1}$$
$$B = 1 + 3e^{2J/kT} + 5e^{6J/kT} + 7e^{12J/kT} + 9e^{20J/kT} + 11e^{30J/kT}$$

The least-squares analysis of magnetic susceptibilities data leads to J = –1.01 cm^{-1}, g = 1.98, and $R = 2.34 \times 10^{-3}$ for **1**; J = –0.54 cm^{-1}, g = 1.99, and $R = 3.19 \times 10^{-4}$ for **3**; J = –0.47 cm^{-1}, g = 1.99, and $R = 3.58 \times 10^{-4}$ for **4**; and J = –1.95 cm^{-1}, g = 2.01, and $R = 1.23 \times 10^{-4}$ for **6**. The small J value indicates very weak antiferromagnetic interactions between the Mn(II) ions in **1**, **3**, and **4**, which may originate from the the long distances of adjacent Mn···Mn. In view of the standard deviation of the obtained values, the zero field splitting should be taken into consideration that can be also responsible for the decrease of the magnetic moment at very low temperatures. This condition is the same for **7** (discussed below).

For **2**, the room temperature value of $\chi_M T$ was found to be 32.7 cm^3 K mol^{-1}, corresponding to eight isolated Mn(II) ions (S = $^5/_2$; g = 2.00). As the temperature is lowered to 2 K, the $\chi_M T$ product continuously decrease to 10.6 cm^3 K mol^{-1}, which suggests that antiferromagnetic interaction is operative. The magnetic susceptibility in the range of 300-2 K obeys the Curie–Weiss law very well with C = 33.47 cm^3 K mol^{-1} and θ = –16.96 K. In **2**, there are three sets of connection between Mn(II) ions according to the structures of **2**. The coupling of two Mn(II) ions in the same triangle utilizing one μ_3-Cl bridge; A Mn(II) ion in the triangle and an apical Mn(II) ion utilizing one $[ptptp]^{2-}$–*N*, *N* bridge; Two Mn(II) ions of different Mn3 triangles utilizing two $[ptptp]^{2-}$–*N*, *N* bridges. The three exchange coupling constant values are negative with an antiferromagnetic state, and the interactions through a double $[ptptp]^{2-}$–*N*, *N* bridges between Mn(II) ions of different triangles are stronger than that with only one $[ptptp]^{2-}$–*N*, *N* bridge between a Mn(II) ion in the triangle and an apical Mn(II) ion in $[\{Mn(\mu\text{-}L)_3\}_2\{Mn_3(\mu_3\text{-}Cl)\}_2](ClO_4)_2\cdot 2MeOH\cdot 6H_2O$.[17] For the one $[ptptp]^{2-}$–*N*, *N* bridge interactions, the average Mn···Mn distance is 4.66 Å and the Mn–N–N–Mn torsion angle is 6.3° in **2**, which is comparable with that in $[\{Mn(\mu\text{-}L)_3\}_2\{Mn_3(\mu_3\text{-}Cl)\}_2](ClO_4)_2\cdot 2MeOH\cdot 6H_2O$.[17]

For **5**, the experimental $\chi_M T$ at room temperature is 14.29 cm^3 K mol^{-1}, which is lower than the spin-only value (17.52 cm^3 K mol^{-1}) expected for four magnetically isolated high-spin Mn(II) ions. As the temperature lowing, the $\chi_M T$ value decreases gradually. In the temperature region above 25 K, a typical paramagnetic Curie–Weiss behavior is observed, with θ = –13.10 K, C = 14.91 cm^3 K mol^{-1}, and $R = 1.15 \times 10^{-4}$. The negative θ value and the decrease of the $\chi_M T$ are indicative of antiferromagnetic interactions in **5**.

The 2D structure of **5** was constructed by using 5-Br-ip ligands to link the 1D Mn(II) ions chains formed through carboxylate, carboxyl oxygen, and $[ptptp]^{2-}$–*N*, *N* bridge. Normally, very weak coupling can be conducted through 5-Br-ip, and thus, the magnetic behaviors show the character of 1D chain in which there are two sets of connection between Mn(II) ions presenting in the ratio of 1 : 1. One connects Mn1 and Mn2 (or Mn4 and Mn5), utilizing two *syn–syn* carboxylate bridges and one μ_2-O bridge from a μ_3-carboxylate group; the other links Mn2 and Mn3 (or Mn3 and Mn4) through one $[ptptp]^{2-}$–*N*, *N* bridge. Thus, the magnetic exchange pathway within the 1D chain can be described as a magnetic Mn(II) chain with periodic $–J_1J_1J_2J_2–$ coupling sequence. In recent papers, Bu et al.,[21] Gao et al.,[22] Du et al.,[23] and Wang et al[24]. have also reported such a sequence. The values of J_1 and J_2 reported by Bu and Gao are negative with an antiferromagnetic state, while the values of J_1 and J_2 reported by Du and Wang are opposite with a ferromagnetic state, where the ferromagnetic exchange coupling may be due to the different coordinated mode of carboxyl group. In order to evaluate the interaction, the least-squares fit of magnetic data using the

theoretical expression proposed by Fisher[25] and extended by Abu-Youssef[26] and others[21-22] was made. The spin Hamiltonian of an alternating $-J_1J_1J_2J_2-$ coupling sequence is:

$$\hat{H} = \sum (J_1 S_{4i+1} S_{4i+2} + J_1 S_{4i+2} S_{4i+3} + J_2 S_{4i+3} S_{4i+4} + J_2 S_{4i+4} S_{4i+5})$$

The magnetic susceptibility is given by equation (2).

$$X_M = \frac{Ng^2\beta^2 S(S+1)}{12kT} \frac{C}{1-u_1^2u_2^2} \quad (2)$$

$$C = 4 + 4u_1 + 4u_2 + 4u_1u_2 + 2u_1^2 + 2u_2^2 + 4u_1^2u_2 + 4u_1u_2^2 + 4u_1^2u_2^2$$

Here $S = {}^5/_2$ and u is the well-known Langevin function, u = coth[$JS(S+1)/kT$] – $kT/JS(S+1)$. The best fitting parameters obtained were $J_1 = -1.27$ cm^{-1}, $J_2 = -1.65$ cm^{-1}, $g = 1.85$, and R = 1.16×10^{-4} for **5**.

For **7**, the room temperature value of $\chi_M T$ was found to be 8.88 cm^3 K mol^{-1}, which is higher than the expected value of 8.75 cm^3 K mol^{-1} for a noninteracting pair of S = $^5/_2$ Mn(II) ions with g = 2.00. An incipient plateau range was observed in the 300–50 K temperature, and then sharply decreases down to a minimum of 3.62 cm^3 K mol^{-1}. The magnetic susceptibility in the range of 300–2 K obeys the Curie–Weiss law very well with $C = 8.97$ cm^3 K mol^{-1}, $\theta = -3.55$ K, and $R = 1.54 \times 10^{-4}$, indicating the overall antiferromagnetic interactions between the Mn(II) ions.

In **7**, the adjacent Mn···Mn distances are 4.7080(6) Å (Mn1–Mn2) and 5.0326(6) Å (Mn2–Mn1A), respectively, and the Mn1–Mn2–Mn1A angle is 140.841(4)°. According to the structures of **7**, it could be presumed that the main magnetic interactions between the Mn(II) ions should happen through the carboxylates and/or [ptptp]$^{2-}$–*N*, *N* bridges whereas the superexchange interactions between the Mn(II) ions through tdc ligands can be ignored because of the long distances of Mn···Mn separations. The antiferromagnetic behaviour of **7** could be suggested to arise from the intra-chain interactions within the 1D helical chain. There are two sets of connection between the metal ions. One connects Mn1 and Mn2, utilizing one carboxylate bridge (*syn-anti*) and one [ptptp]$^{2-}$–*N*, *N* bridge; the other links Mn2 and Mn1A through one [ptptp]$^{2-}$–*N*, *N* bridge. Thus, the magnetic exchange pathway within the helical chain can be described as a magnetic Mn(II) chain with periodic $-J_1J_2J_1J_2-$ coupling sequence. The isotropic spin-exchange Hamiltonian for the alternating chains in **7** can be given as:

$$H = -J_1 \sum S_{2i} S_{2i+1} - J_2 \sum S_{2i+1} S_{2i+2}$$

where J_1 and J_2 represent the alternating exchange constants between Mn1 and Mn2, Mn2 and Mn1A. The molar magnetic susceptibility expression shown in was obtained:[27]

$$X_M = \frac{Ng^2\mu_B^2}{3kT}\left(\frac{1+u_1+u_2+u_1u_2}{1-u_1u_2}\right) \quad (3)$$

with $u_1 = \coth(J_1/kT) - kT/J_1$ and $u_2 = \coth(J_2/kT) - kT/J_2$. Here N is Avogadro's number, g is the Lande´ g factor, β is the electron Bohr magneton, k is the Boltzmann constant. The best fitting parameters obtained were $J_1 = -0.18$ cm^{-1}, $J_2 = -0.1$ cm^{-1}, g = 1.98, and R = 5.9×10^{-4} for **7**. The very small negative J_1 and J_2 values indicate the weak antiferromagnetic interactions in the helical magnetic Mn(II) chains in **7**.[28]

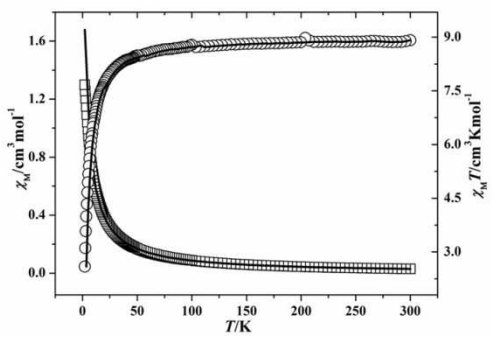

(a)

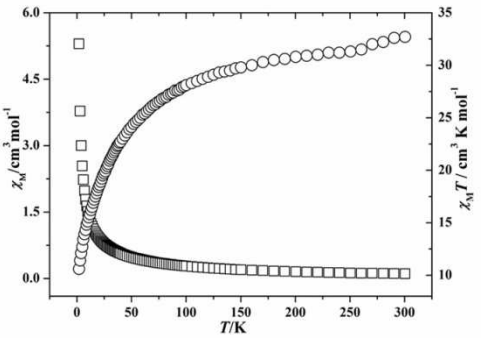

(b)

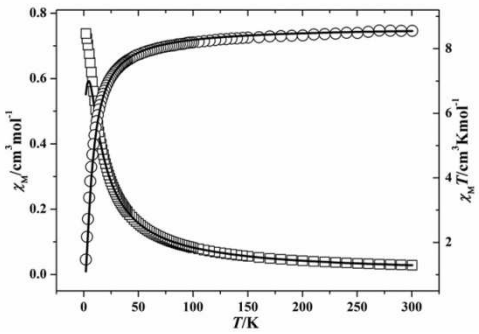

(c)

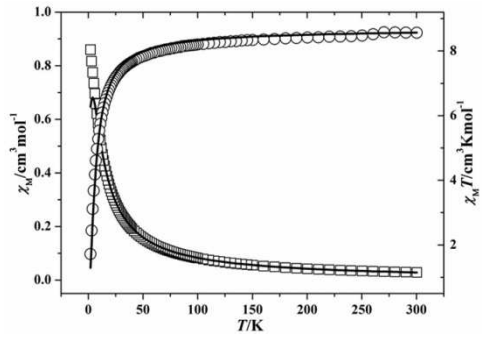

(d)

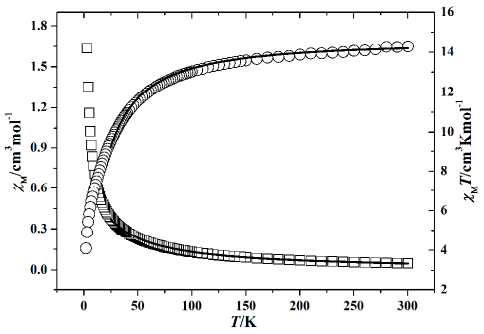

(e)

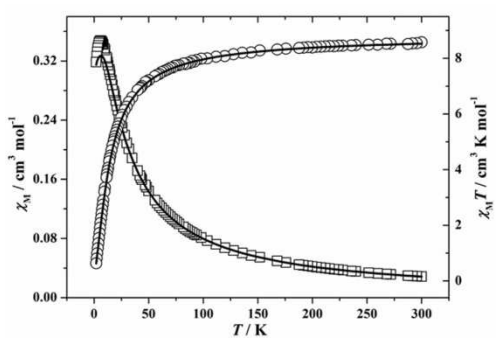

(f)

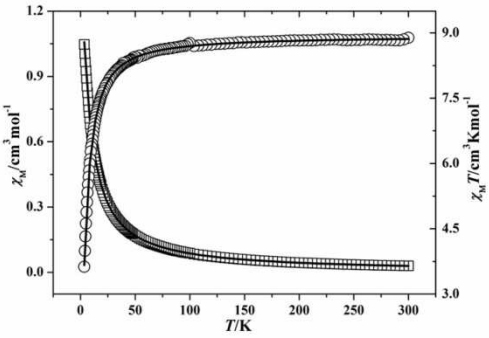

(g)

Fig. 7 Temperature dependence of $\chi_M T$ and χ_M for **1** (a), **2** (b), **3** (c)**,** **4** (d), **5** (e), **6** (f), and **7** (g). Open points are the experimental data, and the solid line represents the best fit obtained from the Hamiltonian given in the text.

Conclusions

In summary, seven Mn(II) CPs have been prepared based on multidentate N-heterocyclic aromatic ligand and bridging carboxylate ligands, in order to further probe the multiple roles of ILs in the hydro/solvothermal synthesis. Experiment result suggests that in hydro/solvothermal synthesis the addition of small amount of [RMI]Br plays a crucial role in the successful syntheses of complexes **2-6**, despite the fact that neither [RMI] cation nor Br^- anion is occluded into the ultimate structure. However, further analysis shows that [RMI]Br may play different roles in the preparation of the five complexes. In **2**, [RMI]Br probably serves as a template directing agent for the formation of $[Mn_3(\mu_3\text{-Cl})]$ triangle cores which are further wrapped by terminal $[Mn(\mu\text{-ptptp})_3]$ units to give octanuclear helicate structures. While in **3-6**, [RMI]Br perhaps serves as a mineralizing agent. Additionally, introducing [RMI]Br into the synthesis process of **7** could obviously improve crystal yield. All these observations declare the combination of hydro/solvothermal and ionothermal methods seems to be a promising synthetic technique for the preparation of functional CPs.

Acknowledgments

This work was funded by the National Natural Science Foundation (21371155; 91022013), Research Found for the Doctoral Program of Higher Education of China (20124101110002) and Henan Science and Technology Agency of China (132300410053).

Notes and references

[a] *College of Chemistry and Molecular Engineering, Zhengzhou University, Zhengzhou 450001, China. E-mail: houhongw@zzu.edu.cn.*
[b] *College of Chemistry and Chemical Engineering, Luoyang Normal University, Luoyang 471022, China.*

† Electronic Supplementary Information (ESI) available: PXRD patterns, TG plots and selected bond lengths and angles for **1**–**7**. See DOI: 10.1039/b000000x/

1 (*a*) W. Reichert, J. Holbrey, K. Vigour, T. Morgan, G. Broker, R. Rogers, *Chem. Commun*., 2006, 4767; (*b*) Z. Fei, T. Geldbach, D. Zhao, P. J. Dyson, *Chem.-Eur. J*., 2006, **12**, 2122; (*c*) E. Parnham, R. Morris, *Acc. Chem. Res*., 2007, **40**, 1005; (*d*) R. Morris, *Chem. Commun*., 2009, 2990; (*e*) E. Ahmed, M. Ruck, *Dalton Trans*., 2011, **40**, 9347; (*f*) D. Freudenmann, S. Wolf, M. Wolff, C. Feldmann, *Angew. Chem. Int. Ed*., 2011, **50**, 11050; (*g*) C. Li, M. Du, *Chem. Commun*., 2011, **47**, 5958.

2…(*a*) E. Cooper, C. Andrews, P. Wheatley, P. Webb, P. Wormald, R. Morris, *Nature*, 2004, **430**, 1012; (*b*) E. Parnham, R. Morris, *J. Am. Chem. Soc*., 2006, **128**, 2204; (*c*) E. Parnham, P. Wheatley, R. Morris, *Chem. Commun*., 2006, 380; (*d*) B. Yonemoto, Z. Linb, F. Jiao, *Chem. Commun*., 2012, **48**, 9132; (*e*) Y. Wei, B. Marler, L. Zhang, Z. Tian, H. Graetscha, H. Gies, *Dalton Trans*., 2012, **41**, 12408.

3 (*a*) K. Jin, X. Huang, L. Pang, J. Li, A. Appel, S. Wherland, *Chem. Commun*., 2002, 2872; (*b*) D. Dybtsev, H. Chun, K. Kim, *Chem. Commun*., 2004, 1594; (*c*) Z. Lin, A. Slawin, R. Morris, *J. Am. Chem. Soc*., 2007, **129**, 4880; (*d*) Z. Lin, D. Wragg, J. Warren, R. Morris, *J. Am. Chem. Soc*., 2007, **129**, 10334; (*e*) J. Zhang, S. Chen, X. Bu, *Angew. Chem., Int. Ed*., 2008, **47**, 5434.

4 (*a*) L. Xu, S. Yan, E. Choi, J. Lee, Y. Kwon, *Chem. Commun*., 2009, 3431; (*b*) H. Ren, T. Ben, E. Wang, X. Jing, M. Xue, B. Liu, Y. Cui, S. Qiu, G. Zhu, *Chem. Commun*., 2010, **46**, 291; (*c*) W. Chen, H. Xu, G. Zhuang, L. Long, R. Huang, L. Zheng, *Chem. Commun*., 2011, **47**, 11933; (*d*) Y. Kang, S. Chen, F. Wang, J. Zhang, X. Bu, *Chem. Commun*., 2011, **47**, 4950.

5 L. Cammarata, S. Kazarian, P. Slater, T. Welton, *Phys. Chem. Chem. Phys*., 2001, **3**, 5192.

6 H. Ma, Z. Tian, R. Xu, B. Wang, Y. Wei, L. Wang, Y. Xu, W. Zhang, L. Lin, *J. Am. Chem. Soc*., 2008, **130**, 8120.

7 D. Du, J. Qin, C. Sun, X. Wang, S. Zhang, P. Shen, S. Li, Z. Su, Y. Lan, *J. Mater. Chem*., 2012, **22**, 19673.

8 (*a*) J. Qin, Y. Jia, H. Li, B. Zhao, D. Wu, S. Zang, H. Hou, Y. Fan, *Inorg. Chem*., 2014, **53**, 685; (*b*) Y. Han, N. Chilton, M. Li, C. Huang, H. Xu, H. Hou, B. Moubaraki, S. Langley, S. Batten, Y. Fan, K. Murray, *Chem.-Eur. J*., 2013, **19**, 6321; (*c*) Y. Jia, H. Li, B. Zhao, Q. Guo, H. Hou, Y. Fan, *Eur. J. Inorg. Chem*., 2013, **3**, 438; (*d*) J. Qin, B. Ma, X. F. Liu, H. L. Lu, X. Y. Dong, S. Q. Zang, H. Hou, *J. Mater. Chem. A*., 2015, **3**, 12690; (*e*) J. Qin, B. Ma, X. F. Liu, H. L. Lu, X. Y. Dong, S. Q. Zang, H. Hou, 2015, *Dalton Trans*., 2015, **44**, 14594.

9 (*a*) C. Janiak, *J. Chem. Soc. Dalton Trans*., 2000, 3885; (*b*) S. Konar, P. Mukherjee, M. Drew, J. Ribas, N. Chaudhuri, *Inorg. Chem*., 2003, **42**, 2545; (*c*) C. Janiak, *Dalton Trans*., 2003, 2781; (*d*) C. Policar, F. Lambert, M. Cesario, I. Morgenstern-Badarau, *Eur. J. Inorg. Chem*., 1999, 2201; (*e*) F. Delgado, N. Kerbellec, C. Ruiz-Perez, J. Cano, F. Lloret, M. Julve, *Inorg. Chem*., 2006, **45**, 1012; (*f*) C. Janiak J. Vieth, *New J. Chem*., 2010, **34**, 2366; (*g*) C. Aakeröy, N. Champness, C. Janiak, *CrystEngComm*, 2010, **12**, 22; (*h*) W. H. Zhang, Q. Liu, J. P. Lang, *Coord. Chem. Rev*., 2015, **293-294**, 187.

10 (*a*) H. Habib, J. Sanchiz, C. Janiak, *Dalton Trans*., 2008, 1734; (*b*) H. Habib, A. Hoffmann, H. Hoppe, C. Janiak, *Dalton Trans*., 2009, 1742; (*c*) H. Habib, J. Sanchiz, C. Janiak, *Inorg. Chim. Acta*., 2009, **362**, 2452; (*d*) M. Meng, D. Zhong, T. Lu, *CrystEngComm*, 2011, **13**, 6794; (*e*) X. Zhang, Y. Wang, Y. Song, E. Gao, *Inorg. Chem*., 2011, **50**, 7284; (*f*) C. Lampropoulos, G. Redler, S. Data, K. Abboud, S. Hill, G. Christou, *Inorg. Chem*., 2010, **49**, 1325; (*g*) L. L. Liu, H. X. Li, L. M. Wan, Z. G. Ren, H. F. Wang, J. P. Lang, *Chem. Commun*., 2011, **47**, 11146; (*h*) H. X. Li, W. Zhao, H. Y. Li, Z. L. Xu, W. X. Wang, J. P. Lang, *Chem. Commun*., 2013, **49**, 4259.

11 (*a*) C. Zhang, C. Janiak, *Z. Anorg. Allg. Chem*., 2001, **627**, 1972; (*b*) Y. Wang, Q. Sun, Q. Yue, A. Cheng, Y. Song, E. Gao, *Dalton Trans*., 2011, **40**, 10966; (*c*) X. Wang, Y. Zhang, X. Zhang, W. Xue, H. Zhou, X. Chen, *CrystEngComm*, 2011, **13**, 4196; (*d*) W. Chen, G. Zhuang, Zhao, X. H. L. Long, R. Huang, L. Zheng, *Dalton Trans*., 2011, **40**, 10237; (*e*) R. Elshaarawy, Y. Lan, C. Janiak, *Inorg. Chim. Acta*., 2013, **401**, 85; (*f*) I. Boldog, K. Domasevitch, I. Baburin, H. Ott, B. Gil-Hernández, J. Sanchiz, C. Janiak, *CrystEngComm*, 2013, **15**, 1235.

12 G. Sheldrick, *SHELXS-97: Program for the Solution of Crystal Structure*; University of Göttingen: Göttingen, Germany, 1997.

13 G. Sheldrick, *SHELXL-97, Program for the Crystal Structure Refinement*; University of Göttingen: Göttingen, Germany, 1997.

14 G. Sheldrick, *SADABS Siemens Area Correction Absorption Program*; University of Göttingen: Göttingen, Germany, 1994.

15 A. Spek, *Implemented as the PLATON Procedure, a Multipurpose Crystallographic Tool*; Utrecht University: Utrecht, The Netherlands, 1998.

16 (*a*) R. Saalfrank, N. Löwa, S. Trummera, G. Sheldrickb, M. Teichertb, D. Stalkec, *Eur. J. Inorg. Chem*., 1998, 559; (*b*) M. Vázquez, M. Bermejo, M. Licchelli, A. González-Noya, R. Pedrido, C. Sangregorio, L. Sorace, A. García-Deibe, J. Sanmartín, *Eur. J. Inorg. Chem*., 2005, 3479; (*c*) A. Zhu, J. Zhang, Y. Lin, X. Chen, *Inorg. Chem*., 2008, **47**, 7389; (*d*) J. Hou, M. Li, Z. Li, S. Zhan, X. Huang, D. Li, *Angew. Chem. Int. Ed*., 2008, **47**, 1711; (*e*) X. Bao, J. Leng, Z. Meng, Z. Lin, M. Tong, M. Nihei, H. Oshio, *Chem.-Eur. J*., 2010, **16**, 6169; (*f*) R. Ishikawa, M. Nakano, A. Fuyuhiro, T. Takeuchi, S. Kimura, T. Kashiwagi, M. Hagiwara, K. Kindo, S. Kaizaki, S. Kawata, *Chem.-Eur. J*., 2010, **16**, 11139; (*g*) S. Romain, J. Rich, C. Sens, T. Stoll, J. Benet-Buchholz, A. Llobet, M. Rodriguez, I. Romero, R. Clerac, C. Mathoniere, C. Duboc, A. Deronzier, M. Collomb, *Inorg. Chem*., 2011, **50**, 8427.

17 X. Bao, W. Liu, J. Liu, S. Gomez-Coca, E. Ruiz, M. Tong, *Inorg. Chem*., 2013, **52**, 1099.

18 (*a*) S. Bourne, J. Lu, A. Mondal, B. Moulton, M. Zaworotko, *Angew. Chem. Int. Ed*., 2001, **40**, 2111; (*b*) M. Eddaoudi, J. Kim, J. Wachter, H. Chae, M. O'Keeffe, O. Yaghi, *J. Am. Chem. Soc*., 2001, **123**, 4368; (*c*) L. Pan, B. Parker, X. Huang, D. Olson, J. Lee, J. Li, *J. Am. Chem. Soc*., 2006, **128**, 4180; (*d*) H. Chun, *J. Am. Chem. Soc*., 2008, ***130***, 800; (*e*) A. Cairns, J. Perman, L. Wojtas, V. Kravtsov, M. Alkordi, M. Eddaoudi, M. Zaworotko, *J. Am. Chem. Soc*., 2008, **130**, 1560; (*f*) L. Ma, L. Wang, D. Lu, S. Batten, J. Wang, *Cryst. Growth Des*., 2009, **9**, 1741; (*g*) L. Ma, L. Wang, Y. Wang, S. Batten, J. Wang, *Inorg. Chem*., 2009, **48**, 915; (*h*) L. Ma, L. Wang, M. Du, S. Batten, *Inorg. Chem*., 2010, **49**, 365; (*i*) M. Du, C. P. Li, C. S. Liu, S. M. Fang, *Coord. Chem. Rev*., 2013, **257**, 1282; (*j*) M. Du, Z. H. Zhang, Y. P. You, X. J. Zhao, *CrystEngComm*, 2008, **10**, 306.

19 (*a*) X. Li, R. Cao, W. Bi, Y. Wang, Y. Wang, X. Li, Z. Guo, *Cryst. Growth Des*., 2005, **5**, 1651; (*b*) L. Ma, L. Wang, J. Hu, Y. Wang, G. Yang, *Cryst. Growth Des*., 2009, **9**, 5334; (*c*) J. Chen, C. Li, M. Du, *CrystEngComm*, 2011, **13**, 1885; (*d*) H. Reinsch, S. Waitschat, N. Stock, *Dalton Trans*., 2013, **42**, 4840; (*e*) A. Schoedel, W. Boyette, L. Wojtas, M. Eddaoudi, M. Zaworotko, *J. Am. Chem. Soc*., 2013, **135**, 14016; (*f*) M. Du, C. Li, M. Chen, Z. Ge, X. Wang, L. Wang, C. Liu, *J. Am. Chem. Soc*., 2014, **136**, 10906; (*g*) C. P. Li, J. Chen, P. W. Liu, M. Du, *CrystEngComm*, 2013, **15**, 9713; (*h*) C. P. Li, J. Chen, Y. H. Mu, M. Du, *Dalton Trans*., 2015, 44, 11109.

20 R. Carlin, *Magnetochemistry*; Springer: Berlin, 1986.

21 J. Zhao, B. Hu, Q. Yang, X. Zhang, T. Hu, X. Bu, *Dalton Trans*., 2010, **39**, 56.

22 (*a*) Y. Wang, Q. Jia, K. Wang, A. Cheng, E. Gao, *Inorg. Chem*., 2010, **49**, 1551; (*b*) X. Zhang, Y. Wang, X. Li, E. Gao, *Dalton Trans*., 2012, **41**, 2026.

23 C. Tian, Z. He, Z. Li, P. Lin, S. Du, *CrystEngComm*, 2011, **13**, 3080.

24 L. Ma, M. Han, J. Qin, L. Wang, M. Du, *Inorg. Chem*., 2012, **51**, 9431.

25 M. Fisher, *Am. J. Phys*., 1964, **32**, 343.

26 (*a*) M. Abu-Youssef, A. Escuer, M. Goher, F. Mounter, G. Reib, R. Vicente, *Angew. Chem. Int. Ed*., 2000, **39**, 1624; (*b*) Y. J. Cano, Journaux, M. Goher, M. Abu-Youssef, F. Mautner, G. Reib, A. Escuer, R. Vicente, *New J. Chem*., 2005, **29**, 306; (*c*) M. Abu-Youssef, M. Drillon, A. Escuer, M. Goher, F. Mautner, R. Vicente, *Inorg. Chem*., 2000, **39**, 5022.

27 R. Cortés, M. Drillon, X. Solans, L. Lezama, T Rojo, *Inorg. Chem*., 1997, **36**, 677.

28 S. Yu, S. Lippard, I. Shweky, A. Bino, *Inorg. Chem*., 1992, **31**, 3502.

Table 1. Crystallographic Data and Structure Refinement Details for **1-7**.

Complexes	**1**	**2**	**3**	**4**	**5**	**6**	**7**
Formula	$C_{17}H_{17}Cl_2Mn_2N_{11}O_4$	$C_{102}H_{86}Cl_4Mn_8N_{66}O_{16}$	$C_{25}H_{21}Mn_2N_{11}O_8$	$C_{26}H_{23}Mn_2N_{11}O_8$	$C_{41}H_{32}Br_3Mn_4N_{11}O_{19}$	$C_{26}H_{21}Mn_2N_{11}O_{10}$	$C_{46}H_{36}Mn_4N_{22}O_{15}S_2$
Formula weight	620.20	3073.52	713.41	727.43	1442.22	757.42	1420.80
Crystal system	Monoclinic	Triclinic	Monoclinic	Monoclinic	Triclinic	Monoclinic	Tetragonal
Space group	*P*2(1)	*P*-1	*P*2(1)/c	*P*2(1)/c	*P*-1	*P*2(1)/c	*P*4(2)/*n*
a (Å)	8.3747(17)	18.489(4)	12.018(2)	12.325(3)	9.766(2)	16.001(3)	24.053(4)
b (Å)	13.005(3)	18.973(4	16.358(3)	16.317(3)	13.320(3)	10.142(2)	24.053(4)
c (Å)	10.693(2)	20.929(4)	15.613(3)	15.585(3)	22.662(5)	19.287(4)	9.307(3)
α(°)	90	112.87(3)	90	90	89.07(3)	90	90
β(°)	90.68(3)	100.08(3)	106.11(3)	104.60(3)	88.35(3)	101.27(3)	90
γ(°)	90	99.89(3)	90	90	82.39(3)	90	90
V ($Å^3$)	1164.5(4)	6423(2)	2948.8(10)	3033.2(11)	2920.7(10)	3069.5(11)	5385(2)
Z	2	2	4	4	2	4	4
D_c (g/cm^3)	1.769	1.440	1.607	1.593	1.558	1.639	1.753
Abs coeff/mm^{-1}	1.365	0.915	0.925	0.901	2.963	0.898	1.086
F(000)	624	2792	1448	1480	1344	1536	2872
θ range for data collection (°)	2.47/25.00	1.80/25.50	2.16/25.50	2.12/25.50	2.10/25.50	2.15/25.50	2.35/25.50
Data/restraints/parameters	3920 / 7 / 325	23850 / 0 / 1621	5326 / 6 / 415	5431 / 6 / 425	10550 / 334 / 668	5597 / 96 / 439	5015 / 12 / 406
GOF	1.026	1.020	1.042	1.043	1.015	1.087	1.045
Flack parameter	0.07(2)	None	None	None	None	None	None
R [$I > 2\sigma(I)$]	$R_1 = 0.0377$ $wR_2 = 0.0833$	$R_1 = 0.0978$ $wR_2 = 0.2917$	$R_1 = 0.0821$ $wR_2 = 0.1618$	$R_1 = 0.0792$ $wR_2 = 0.2122$	$R_1 = 0.0581$ $wR_2 = 0.1532$	$R_1 = 0.0594$ $wR_2 = 0.1487$	$R_1 = 0.0486$ $wR_2 = 0.1227$
R (all data)	$R_1 = 0.0399$ $wR_2 = 0.0852$	$R_1 = 0.1353$ $wR_2 = 0.3289$	$R_1 = 0.1421$ $wR_2 = 0.1940$	$R_1 = 0.0974$ $wR_2 = 0.2309$	$R_1 = 0.0725$ $wR_2 = 0.1637$	$R_1 = 0.0679$ $wR_2 = 0.1564$	$R_1 = 0.0732$ $wR_2 = 0.1380$

[5] $R = [\sum || F_0| - |F_c|| / \sum |F_0|]$, $R_W = \sum_W [| F_0^2 - Fc^2 |^2 / \sum_W (|F_w|^2)^2]^{1/2}$

Influence of ionic liquids on the syntheses and structures of Mn(II) coordination polymers based on multidentate N-heterocyclic aromatic ligand and bridging carboxylate ligands

Jian-Hua Qin,[a,b] Hua-Rui Wang,[a,b] Qi Pan,[a] Shuang-Quan Zang,[a] Hongwei Hou,*[a] and Yaoting Fan[a]

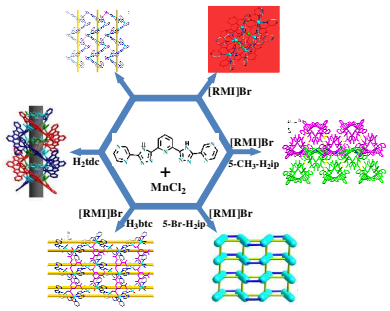

[RMI]Br probably serves as a template directing agent for the formation of cluster helicate in **2**, while serves as a mineralizing agent in **3-6**. Additionally, [RMI]Br could obviously improve crystal yield of **7**.